UCLA

Title

Radio-pathomic estimates of cellular growth kinetics predict survival in recurrent glioblastoma

Authors

Oshima, Sonoko

Yao, Jingwen

Bobholz, Samuel

et al.

Peer reviewed

Taylor & Francis
Taylor & Francis Group

RESEARCH ARTICLE

OPEN ACCESS · Check for updates

Radio-pathomic estimates of cellular growth kinetics predict survival in recurrent glioblastoma

Sonoko Oshima[a,b], Jingwen Yao[a,b,c] (ID), Samuel Bobholz[d], Raksha Nagaraj[a,b], Catalina Raymond[a,b], Ashley Teraishi[a,b], Anna-Marie Guenther[a,c], Asher Kim[a,c], Francesco Sanvito[a,b], Nicholas S Cho[a,b,c,e], Blaine S C Eldred[f] (ID), Jennifer M Connelly[g], Phioanh L Nghiemphu[f,h], Albert Lai[f,h], Noriko Salamon[b], Timothy F Cloughesy[f,h], Peter S LaViolette[d,i,j] (ID) and Benjamin M Ellingson*[a,b,c,k,l] (ID)

aUCLA Brain Tumor Imaging Laboratory (BTIL), Center for Computer Vision & Imaging Biomarkers, University of California Los Angeles, Los Angeles, CA 90024, USA; bDepartment of Radiological Sciences, David Geffen School of Medicine, University of California Los Angeles, Los Angeles, CA 90024, USA; cDepartment of Bioengineering, Henry Samueli School of Engineering & Applied Science, University of California Los Angeles, Los Angeles, CA 90024, USA; dDepartment of Radiology, Medical College of Wisconsin, Milwaukee, WI 53226, USA; eMedical Scientist Training Program, David Geffen School of Medicine, University of California Los Angeles, Los Angeles, CA 90024, USA; fUCLA Neuro-Oncology Program, David Geffen School of Medicine, University of California Los Angeles, Los Angeles, CA 90024, USA; gDepartment of Neurology, Medical College of Wisconsin, Milwaukee, WI 53226, USA; hDepartment of Neurology, David Geffen School of Medicine, University of California Los Angeles, Los Angeles, CA 90024, USA; iDepartment of Biophysics, Medical College of Wisconsin, Milwaukee, WI 53226, USA; jDepartment of Biomedical Engineering, Medical College of Wisconsin, Milwaukee, WI 53226, USA; kDepartment of Psychiatry & Biobehavioral Sciences, David Geffen School of Medicine, University of California Los Angeles, Los Angeles, CA 90024, USA; lDepartment of Neurosurgery, David Geffen School of Medicine, University of California Los Angeles, Los Angeles, CA 90024, USA

ABSTRACT

Aim: A radio-pathomic machine learning (ML) model has been developed to estimate tumor cell density, cytoplasm density (Cyt) and extracellular fluid density (ECF) from multimodal MR images and autopsy pathology. In this multicenter study, we implemented this model to test its ability to predict survival in patients with recurrent glioblastoma (rGBM) treated with chemotherapy.

Methods: Pre- and post-contrast T_1-weighted, FLAIR and ADC images were used to generate radio-pathomic maps for 51 patients with longitudinal pre- and post-treatment scans. Univariate and multivariate Cox regression analyses were used to test the influence of contrast-enhancing tumor volume, total cellularity, mean Cyt and mean ECF at baseline, immediately post-treatment and the pre- and post-treatment rate of change in volume and cellularity on overall survival (OS).

Results: Smaller Cyt and larger ECF after treatment were significant predictors of OS, independent of tumor volume and other clinical prognostic factors (HR = 3.23×10^{-6}, p < 0.001 and HR = 2.39×10^{5}, p < 0.001, respectively). Both post-treatment volumetric growth rate and the rate of change in cellularity were significantly correlated with OS (HR = 1.17, p = 0.003 and HR = 1.14, p = 0.01, respectively).

Conclusion: Changes in histological characteristics estimated from a radio-pathomic ML model are a promising tool for evaluating treatment response and predicting outcome in rGBM.

1. Introduction

Glioblastoma (GBM) is a highly aggressive cancer with a notably poor prognosis and almost all GBMs recur after initial therapy [1,2]. Standard treatment options for recurrent glioblastoma (rGBM) are limited [3,4], with cytotoxic therapies like lomustine used routinely and new therapies including anti-angiogenic treatments and immunotherapy being tested in clinical trials. Consequently, the identification of noninvasive biomarkers for predicting patient responses to new therapies is

imperative. Improved overall survival (OS), radiologic progression-free survival (PFS) and objective response rate (ORR) are all considered valid end points in brain tumor clinical trials [5,6] with the use of the Response Assessment in Neuro-Oncology (RANO) criteria [7–10], which is largely dependent on the use of contrast enhancement on post-contrast T_1-weighted images as a surrogate for tumor burden [11–14]. However, contrast-enhancing tumor volume may not always reflect the true disease burden. Pseudo-progression can occur after

---

CONTACT Benjamin M. Ellingson Tel.: +310-481-7572; ✉ bellingson@mednet.ucla.edu

Supplemental data for this article can be accessed at https://doi.org/10.1080/20450907.2024.2415285

radiotherapy or certain immunotherapies, which can cause new or progressed contrast enhancement on MR images due to a local tissue response that includes inflammation, edema and altered vascular permeability [15,16]. On the other hand, anti-angiogenic therapies can cause pseudo-response, resulting in a rapid decline in contrast enhancement with a high 6-month PFS, but has relatively little influence on OS [15]. Hence, there are inherent limitations in using contrast-enhanced volumes to determine the actual presence or progression of tumors and imaging methods that can detect the underlying pathology more accurately are needed.

Given the challenges associated with obtaining biopsy samples from brain tumors, non-invasive imaging techniques that can provide histologic information would be particularly valuable. Recently, a machine-learning based radio-pathomic mapping approach was developed to estimate tumor cell density, cytoplasm (Cyt) and extracellular fluid density (ECF) by training the algorithm on anatomic MR images and corresponding post-mortem autopsy tissue samples from patients with GBM, *IDH* mutant gliomas, brain metastases and lymphoma [17–19]. In the current study, we extend use of this model to test whether changes in histological characteristics can be used as a response biomarker for predicting survival in rGBM patients treated with cytotoxic chemotherapies.

2. Materials & methods

2.1. Patients

In this retrospective study, we included consecutive patients with first or second rGBM treated at our institution between 2004 and 2022. These patients underwent chemotherapy using lomustine, temozolomide, or carboplatin. All patients provided written, informed consent to be included in our Neuro Oncology Database, which has received approval from our IRB (IRB-10-0655, reviewed by UCLA Medical IRB #2). The inclusion criteria for patient selection were as follows: a minimum of three pre-treatment scans obtained before initiating the next line of therapy; recurrence occurring at least 3 months after the completion of radiation therapy (RT); the earliest pre-treatment scan conducted at least two weeks post-RT completion; a baseline scan within 1 month before the start of second or third line treatment; no anti-angiogenic therapy administered during the assessment; and no surgical or therapeutic interventions carried out before RANO-defined disease progression [8] (Figure 1).

2.2. MR data acquisition

MR images were obtained on 1.5- or 3-T scanners at our institution or external institutions (Siemens Healthcare, Erlangen, Germany; GE HealthCare, Waukesha, United States; Phillips Healthcare, Best, Netherlands; Toshiba Medical, Tokyo, Japan). Patients received pre- and post-contrast T_1-weighted, FLAIR and diffusion weighted images. Detailed parameters are shown in the Supplementary Table S1.
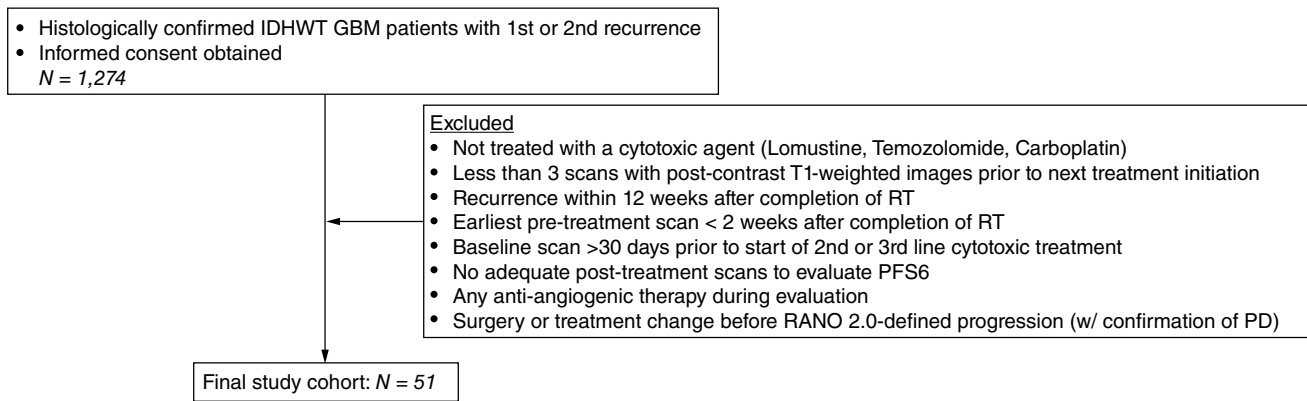
2.3. Radio-pathomic mapping

A previously developed radio-pathomic mapping algorithm trained and tested on imaging and histology acquired at the Medical College of Wisconsin was applied to MRI data acquired at University of California, Los Angeles. Pre- and post-contrast enhanced T_1-weighted, FLAIR and ADC images were fed into the algorithm, which then generated whole brain images of cell density, Cyt and ECF (Figure 2). The details of the algorithm, including training and testing, are described in detail elsewhere [17].

2.4. Feature extraction

Contrast enhancing tumor volume was estimated NS-HGlio v.2.0 deep learning algorithm (Neosoma Inc, MA, United States) [20], supplemented by manual adjustments as needed. For timepoints in which this method was unsuccessful, semi-automated segmentation of enhancing tumor were performed using Analysis of Functional Neuroimages software (AFNI, https://afni.nimh.nih.gov) [21] by manually identifying the relative tumor region and determining thresholds on the subtraction maps, which were created by subtracting pre-contrast T_1-weighted images from post-contrast T_1-weighted images as described previously [22]. These segmentations were then edited by a neuroradiologist (S.O., with 11-year-experience in neuroradiology). Total tumor cellularity was estimated by summing the cell density per voxel on radio-pathomic maps across the entirety of the enhancing tumor volume. Additionally, mean Cyt and ECF within the contrast-enhanced tumor lesions were calculated and used for subsequent analyses.

2.5. Statistical analysis

First, the prognostic value of various imaging features at baseline along with the immediate post-treatment scan (2 weeks–2 months after treatment start) were evaluated. We conducted univariate Cox regression analysis to assess the effect of tumor volume, total cellularity, mean Cyt and mean ECF on OS from the start of chemotherapy. We also performed multivariate Cox regression analysis to adjust for age, sex, *MGMT* promoter methylation status, number of recurrences, concomitant RT and MRI parameters (echo time [TE] for T_2-weighted FLAIR images, whether above or below 100 ms and whether T_1-weighted images were

- Histologically confirmed IDHWT GBM patients with 1st or 2nd recurrence
- Informed consent obtained
  N = 1,274

Excluded
- Not treated with a cytotoxic agent (Lomustine, Temozolomide, Carboplatin)
- Less than 3 scans with post-contrast T1-weighted images prior to next treatment initiation
- Recurrence within 12 weeks after completion of RT
- Earliest pre-treatment scan < 2 weeks after completion of RT
- Baseline scan >30 days prior to start of 2nd or 3rd line cytotoxic treatment
- No adequate post-treatment scans to evaluate PFS6
- Any anti-angiogenic therapy during evaluation
- Surgery or treatment change before RANO 2.0-defined progression (w/ confirmation of PD)

Final study cohort: *N = 51*

Figure 1. CONSORT diagram.
PFS: Progression free survival; RANO: Response assessment in neuro-oncology; RT: Radiation therapy; PD: Progressive disease.

acquired with inversion recovery [IR], details provided in the following section). For total cellularity, ECF and Cyt, tumor volume at baseline or 1st post-treatment scan was included as an additional covariate to evaluate their added prognostic value. Log-rank comparison of Kaplan-Meier curves of patients stratified based on the optimal threshold value of different imaging features were also performed. The optimal threshold of tumor volume, total cellularity, mean Cyt and mean ECF were determined by calculating the log-rank Mantel-Haenszel hazard ratio (HR) and *p*-values at all possible thresholds, similar to previous approaches [23].

In addition to baseline and immediate post-treatment exams, the time rate of change in these parameters before and after the start of treatment were also evaluated. Pre-treatment rates of change were estimated from measurements obtained prior to treatment initiation, while post-treatment rates were estimated from data available post-treatment within the first 6 months after treatment, similar to procedures described previously [24]. The change in the rate of these variables were determined by calculating the difference in rates between pre- and post-treatment time points. Univariate Cox regression analysis was performed to assess the effect on OS for continuous values of pre-treatment rates of change, post-treatment rates of change and the change in rates after treatment for measures of tumor volume, total cellularity, mean Cyt and mean ECF. Multivariate Cox regression analysis was performed to adjust for age, sex, *MGMT* methylation status, number of recurrences, RT and the baseline value of the metric of interest. For log-rank analysis, patients were divided based on the optimal threshold value of pre-treatment rates of change, post-treatment rates of change and the change in these rates after treatment for both tumor volume and total cellularity. The Kaplan-Meier survival curves of the stratified patient groups were compared using a log-rank test.

Lastly, we evaluated the effect of acquisition parameter heterogeneity on the resulting radio-pathomic maps by performing quality assessments via visual inspection of the resulting maps. We observed that the appearance of radio-pathomic maps derived from FLAIR and T_1-weighted images acquired with significantly different parameters showed variation across different timepoints (Supplementary Figure S1). To mitigate bias caused by the acquisition heterogeneity, we included TE of FLAIR acquisition ($> = 100$ ms or <100 ms) and T_1-weighted images acquisition sequence (with or without IR) as additional covariates in the cross-sectional multivariate Cox regression analyses. For analysis involving the time rate of change, we further performed a supplementary analysis of the derived radio-pathomic maps with a more homogeneous dataset by excluding timepoints classified as a smaller subset based on FLAIR and T_1-weighted images acquisition parameters for each subject, in addition to the main analysis using all timepoints from all subjects. This analysis was only performed with sufficient timepoints remained after the exclusion.

p-value below 0.05 was considered as statistically significant. We performed statistical analyses using Prism (v8.2.0; GraphPad Software, CA, USA) and MATLAB (release 2019b, Mathworks, Inc., MA, USA). The time interval between the start of therapy and the date of death from any cause was used to calculate OS. Otherwise, OS was censored at the last clinical follow-up date.

3. Results

A total of 51 patients met the inclusion criteria out of 1,274 rGBM patients available (age, 60.9 ± 9.2 [mean ± standard deviation]; 30 males). Among them, 4 patients had their first and second recurrences evaluated. As a result, 55 datasets were processed, comprising 42 cases following the first progression and 13 cases
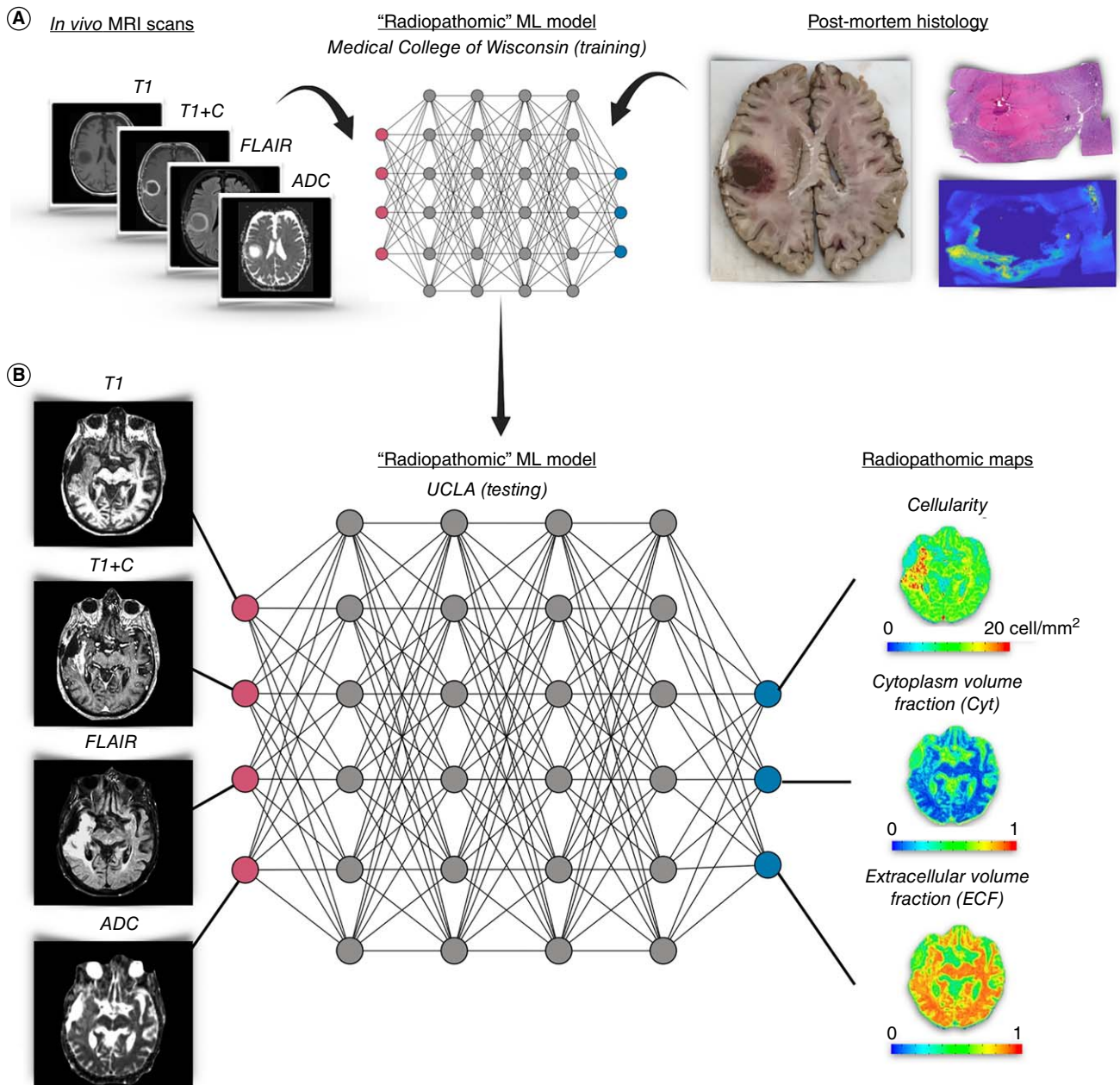
Figure 2. Overview of the methods of this study. **(A)** Pre- and post-contrast T$_1$-weighted, FLAIR and ADC images were used to train a "radiopathomic" machine learning (ML) model to predict histological characteristics using post-mortem brain tissue. **(B)** This model was then applied to an independent cohort of patients to testimate cellularity, cytoplasm volume fraction (Cyt) and extracellular volume fraction (ECF) before and after cytotoxic therapy.

following the second recurrence. The range of OS was 42–2085 days from the start of treatment, with a median of 479.3 days. Figure 3 shows representative cases of tumors that responded and those that did not respond to chemotherapy. Cellularity maps showed clear hyper-cellularity within contrast-enhancing tumor areas, but importantly areas of hypercellularity were also observed beyond areas of contrast enhancement in some cases (Supplementary Figure S2). Additional patient character-istics are described in Table 1.

3.1. Cross-sectional evaluation

A total of 54 datasets were available to evaluate the influence of baseline characteristics and 50 datasets were available to evaluate the characteristics at the 1st post-treatment time point. Univariate Cox regression revealed that baseline enhancing tumor volume and total cellularity at both baseline and the 1st follow-up after treatment were associated longer OS (Table 2, volume at baseline: $p < 0.001$, HR = 1.08, 95% CI 1.04–1.13; volume at 1st post-treatment: $p < 0.001$, HR = 1.07, 95% CI 1.04–
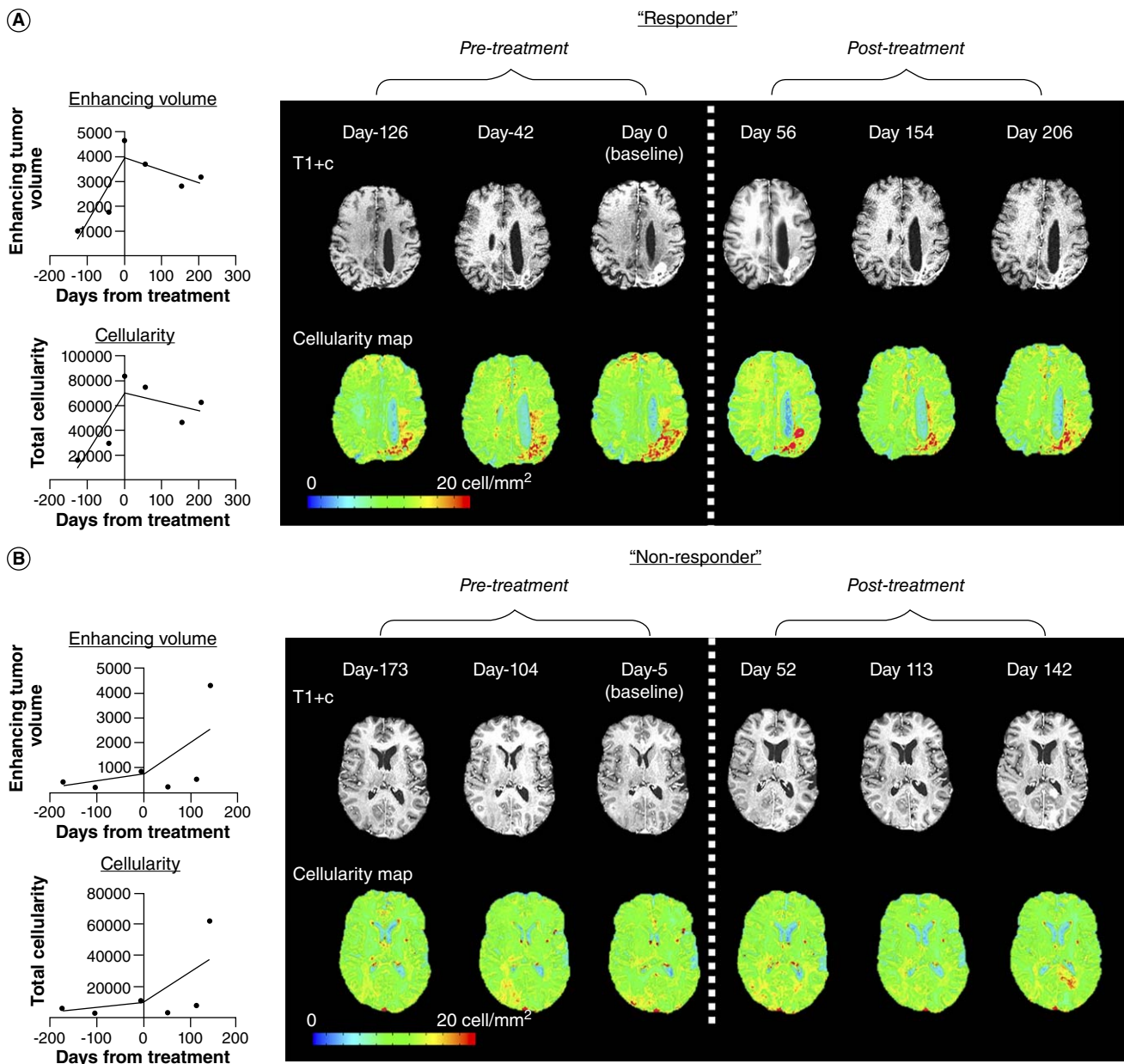
Figure 3. Representative cases: **(A)** A 68-year-old female *IDH* wild-type glioblastoma patient who responded to chemotherapy as evidenced by a reduction in enhancing tumor volume and cellularity after the initiation of chemotherapy. **(B)** A 64-year-old female *IDH* wild-type glioblastoma patient who did not respond to chemotherapy and had increasing volume of enhancing tumor and cellularity after treatment.

1.10; total cellularity at baseline: $p < 0.001$, HR = 1.005, 95% CI 1.002–1.007; total cellularity at 1st post-treatment: $p < 0.001$, HR = 1.004, 95% CI 1.002–1.005). Additionally, larger ECF and smaller Cyt at the 1st post-treatment time point were also associated with longer OS (ECF: $p = 0.001$, HR = 2.43×10^{-5}, 95% CI 3.94×10^{-8}–0.02; Cyt: $p = 0.001$, HR = 3.01×10^4, 95% CI $61.23–1.48 \times 10^7$).

After adjusting for *MGMT* methylation, number of previous recurrences and use of concomitant RT, tumor volume at both the baseline and the 1st post-treatment time point negatively impacted OS (baseline:

$p = 0.01$, HR = 1.07, 95% CI 1.01–1.14; 1st post-treatment: $p < 0.001$, HR = 1.07, 95% CI 1.03–1.11). Additionally, both larger ECF and smaller Cyt at the 1st post-treatment time point were also associated with longer OS (ECF: $p < 0.001$, HR = 3.23×10^{-6}, 95% CI 2.91×10^{-9}–0.004; Cyt: $p < 0.001$, HR = 2.39×10^5, 95% CI $275.09–2.08 \times 10^8$).

Log-rank analyses applied to optimized thresholds suggested enhancing tumors <5.5 cc at baseline (Figure 4A, Log-Rank test; $p = 0.001$, median OS = 470.5 vs 314 days) and enhancing tumors <19 cc at the 1st post-treatment follow-up were associated with a longer

Table 1. Patient characteristics.

	n = 51[a]
Age, y (mean ± SD)	60.9 ± 9.2
Sex (M/F)	30/21
MGMT promoter (methylated/unmethylated/unknown)	24/22/5
Number of recurrences (1st/2nd)	42/13
Treatment	
Lomustine	18
Temozolomide	18
Carboplatin	2
Lomustine + RT	6
Temozolomide + RT	8
Carboplatin + RT	1
Carboplatin + pembrolizumab	1

[a]Four patients were analyzed for both 1st and 2nd recurrences.
RT: Radiation therapy; SD: Standard deviation.

OS (Figure 4C, $p < 0.001$, median OS = 470.5 vs 171 days). Additionally, cellularity $<1.7 \times 10^9$ cells at baseline (Figure 4B, $p < 0.001$, median OS = 467 vs 250 days) and cellularity $<2.0 \times 10^9$ cells at the 1st post-treatment scan were associated with longer OS (Figure 4D, $p < 0.001$, median OS = 508 vs 222 days). Mean ECF $>24.9\%$ at the first 1st post-treatment time point (Figure 4E, $p < 0.001$, median OS = 805 vs 336.5 days) and mean Cyt $<73.5\%$ at the 1st post- treatment time point were also associated with longer OS (Figure 4F, $p < 0.001$, median OS = 632.5 vs 307 days).

3.2. Rate of change in enhancing volume & mean cellularity

A total of 52 datasets were available for investigation into the impact of the rate of change in enhancing volume and cellularity on survival. Univariate analysis indicated that lower pre-treatment enhancing tumor growth rate, lower post-treatment enhancing tumor growth rate and a larger decrease in volumetric growth rate after treatment were associated with longer OS (Table 3, pre-treatment growth rate: $p < 0.001$, HR = 3209.3, 95% CI 36.38–2.83×10^5; post-treatment growth rate: $p < 0.001$, HR = 26.16, 95% CI 5.31–128.79; change in growth rate: $p < 0.001$, HR = 16.27, 95% CI 3.54–74.77). Similarly, the pre-treatment rate of change, post-treatment rate of change and difference in the rate of change in total tumor cellularity within the enhancing tumor after treatment were associated with prolonged OS (pre-treatment growth rate: $p < 0.001$, HR = 1.70, 95% CI 1.29–2.25; post-treatment growth rate: $p < 0.001$, HR = 1.22, 95% CI 1.11–1.34; change in growth rate: $p = 0.006$, HR = 1.17, 95% CI 1.05–1.31).

Multivariable Cox regression controlling for *MGMT* methylation, number of recurrences, use of RT and baseline measurements confirmed that lower post-treatment growth rate and larger decrease in enhancing vol-

umetric growth rate was associated with longer OS (post-treatment growth rate: $p < 0.001$, HR = 16.91, 95% CI 3.41–83.81; change in growth rate: $p = 0.002$, HR = 12.00, 95% CI 2.49–57.90). Additionally, a lower post-treatment rate of change in total tumor cellularity and larger decrease in the rate of change in cellularity with respect to pre-treatment rates were associated with a significant survival advantage (post-treatment growth rate: $p = 0.003$, HR = 1.17, 95% CI 1.05–1.30; change in growth rate: $p = 0.01$, HR = 1.14, 95% CI 1.03–1.27). Of note, pre-treatment enhancing tumor growth rate and pre-treatment rates of change in total tumor cell density were not statistically significant after accounting covariates ($p = 0.25$).

Log-rank analyses applied at the optimal thresholds show survival advantages in patients with a pre-treatment enhancing tumor volumetric growth rate <0.03 cc/day (Figure 5A; $p = 0.005$; median OS = 467 vs 297 days), post-treatment growth rates <0.15 cc/day ($p < 0.001$, median OS = 470.5 vs 161.5 days) and decrease in growth rate $<+0.1$ cc/day ($p < 0.001$, median OS = 467 vs 167 days). Similarly, log-rank analyses applied at the optimal thresholds confirmed that pre-treatment rate of change in tumor cellularity $<4.9 \times 10^7$ cells/day (Figure 5B; $p = 0.003$, median OS = 470.5 vs 317 days), post-treatment rate of change in tumor cellularity $<3.0 \times 10^7$ cells/day ($p < 0.001$, median OS = 464 vs 156 days) and change in the cellularity growth rate $<+1.7 \times 10^7$ cells/day ($p = 0.004$, median OS = 442.5 vs 180 days) were significantly associated with a significant survival advantage.

During quality control evaluation of the resulting radio-pathomic maps, we noticed that some time points appeared to show erroneously high cell density throughout the brain. After investigation, this appeared to be related to variability in the TE of the FLAIR images and use of IR of the T_1-weighted images. Therefore, we conducted a sub-analysis on cases using only the time points with homogeneous acquisition parameters. After removing problematic time points, 40 datasets were available to estimate pre-treatment growth rate parameters, 47 datasets were available for evaluation of post-treatment growth rate parameters and 39 datasets had both pre- and post-treatment data available for evaluation of growth rate changes. Results of this sub-analysis were similar to multivariate Cox regression and log-rank analyses applied to the entire dataset (Supplementary Figure S3 & Supplementary Table S3).

4. Discussion

Identification of the early treatment response and the time of treatment failure continues to be important

Table 2. Results of cox regression analysis in cross-sectional study.

	Univariate analysis		Multivariate analysis	
	Hazard ratio (95% CI)	p-value	Hazard ratio (95% CI)	p-value
Volume (per 1 cc)				
Baseline scan	1.08 (1.04–1.13)	<0.001***	1.07 (1.01–1.14)	0.01*
1st post-treatment scan	1.07 (1.04–1.10)	<0.001***	1.07 (1.03–1.11)	<0.001***
Total cellularity (per 10^7 cells)				
Baseline scan	1.005 (1.002–1.007)	<0.001***	1.005 (0.998–1.01)	0.14
1st post-treatment scan	1.004 (1.002–1.005)	<0.001***	1.003 (0.995–1.01)	0.44
Mean ECF (per 1 unit)				
Baseline scan	0.10 (0.0004–27.55)	0.42	0.09 (8.01×10^{-5}–112.29)	0.51
1st post-treatment scan	2.43×10^{-5} (3.94×10^{-8}–0.02)	0.001***	3.23×10^{-6} (2.91×10^{-9}–0.004)	<0.001***
Mean Cyt (per 1 unit)				
Baseline scan	1.37 (0.26–7.26)	0.71	0.81 (0.10–6.67)	0.84
1st post-treatment scan	3.01×10^4 (61.23–1.48×10^7)	0.001***	2.39×10^5 (275.09–2.08×10^8)	<0.001***

Adjusting for age, sex, *MGMT* methylation, number of recurrences, radiation therapy, TE of FLAIR acquisition (> = 100 ms or <100 ms) and T_1-weighted acquisition sequence (with or without inversion recovery).
For Total cellularity, ECF and Cyt, baseline (or 1st post-Tx) tumor volume was also included as a covariate.
CI: Confidence interval; Cyt: Cytoplasm fraction; ECF: Extracellular fraction. *$P < 0.05$; **$P < 0.01$; ***$P < 0.001$
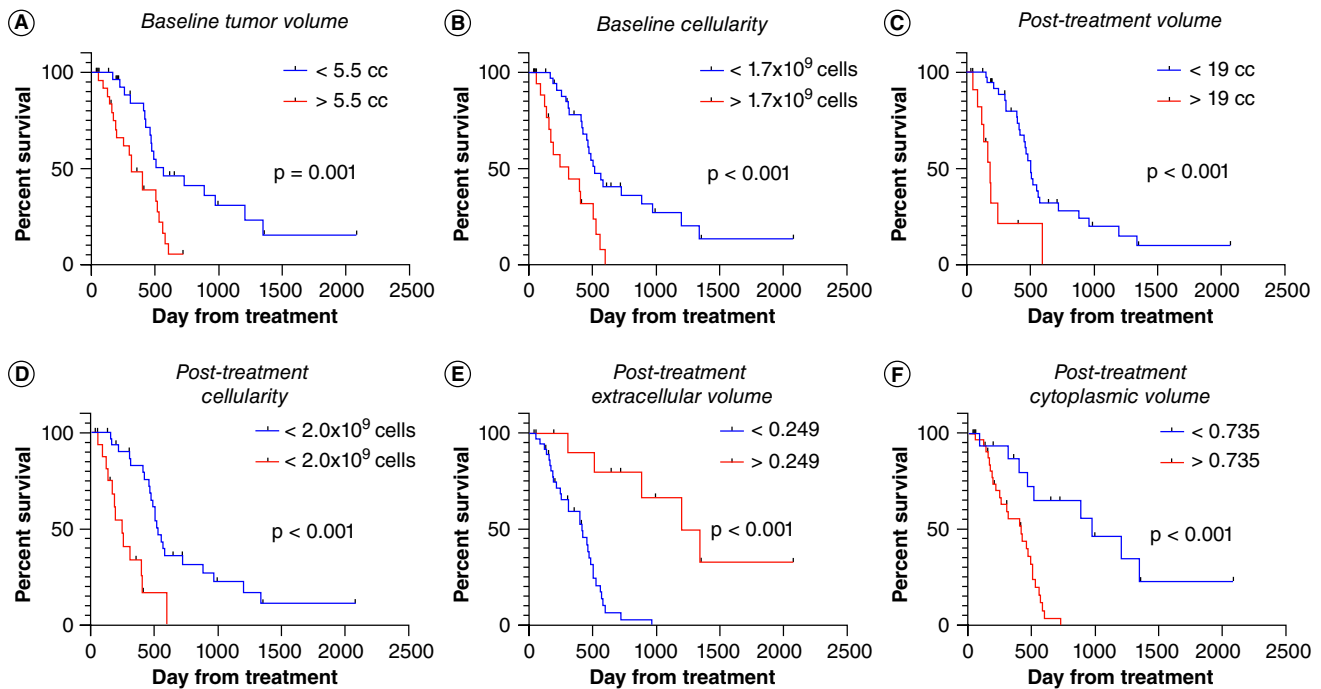
Figure 4. Kaplan-Meier curves for overall survival at baseline and first post-treatment follow-up. Patients with smaller enhancing tumor volume and total cellularity at baseline **(A & B)** and 1st post-treatment scans **(C & D)**, as well as those with smaller Cyt and larger ECF at the 1st post-treatment scan **(E & F)**, demonstrated significantly longer OS.

factors for drug development and clinical care in glioblastoma. While anatomic MRI parameters have been used for decades to describe response to a variety of therapies, MR characteristics can be non-specific and lead to ambiguity in the interpretation of the underlying biological or structural changes. To overcome these issues, a radio-pathomic machine learning model was developed to relate MRI characteristics with the underlying cellular characteristics based on post-mortem human tissue and *in vivo* MRI scans prior to death[28]. Recent multi-institutional data using stereotactic biopsies have verified that these radio-pathomic maps accurately estimate cellularity within various areas of tumor [18], suggesting this approach might provide the much needed clarity into the true biologic changes in the tumor associated with therapeutic perturbation.

We chose to evaluate the use of cytotoxic chemotherapies with or without radiotherapy in recurrent glioblastoma using radio-pathomic maps to benchmark performance of this biomarker in a well-characterized class of

Table 3. Results of cox regression analysis in growth rate study.

	Univariate analysis		Multivariate analysis	
	Hazard ratio (95% CI)	*p*-value	Hazard ratio (95% CI)	*p*-value
Volume (cc/day)				
Pre-treatment growth rate	3209.3 (36.38–2.83 × 10^5)	<0.001***	8993.3 (0.11–7.56 × 10^8)	0.12
Post-treatment growth rate	26.16 (5.31–128.79)	<0.001***	16.91 (3.41–83.81)	<0.001***
Change in growth rate	16.27 (3.54–74.77)	<0.001***	12.00 (2.49–57.90)	0.002**
Total cellularity (10^{7}cells/day)				
Pre-treatment growth rate	1.70 (1.29–2.25)	<0.001***	1.48 (0.76–2.87)	0.25
Post-treatment growth rate	1.22 (1.11–1.34)	<0.001***	1.17 (1.05–1.30)	0.003**
Change in growth rate	1.17 (1.05–1.31)	0.005**	1.14 (1.03–1.27)	0.01*
Total cellularity after excluding timepoints with different MR parameters (10^{7}cells/day)				
Pre-treatment growth rate	1.15 (0.81–1.62)	0.43	0.78 (0.48–1. 26)	0.31
Post-treatment growth rate	1.30 (1.15–1.46)	<0.001***	1.21 (1.07–1.38)	0.002**
Change in growth rate	1.27 (1.11–1.44)	<0.001***	1.20 (1.06–1.37)	0.005**

Adjusting for age, sex, *MGMT* methylation, number of recurrences, radiation therapy and baseline values.
CI: Confidence interval. *$P < 0.05$; **$P < 0.01$; ***$P < 0.001$.

Enhancing tumor growth rate & cellular rate of change
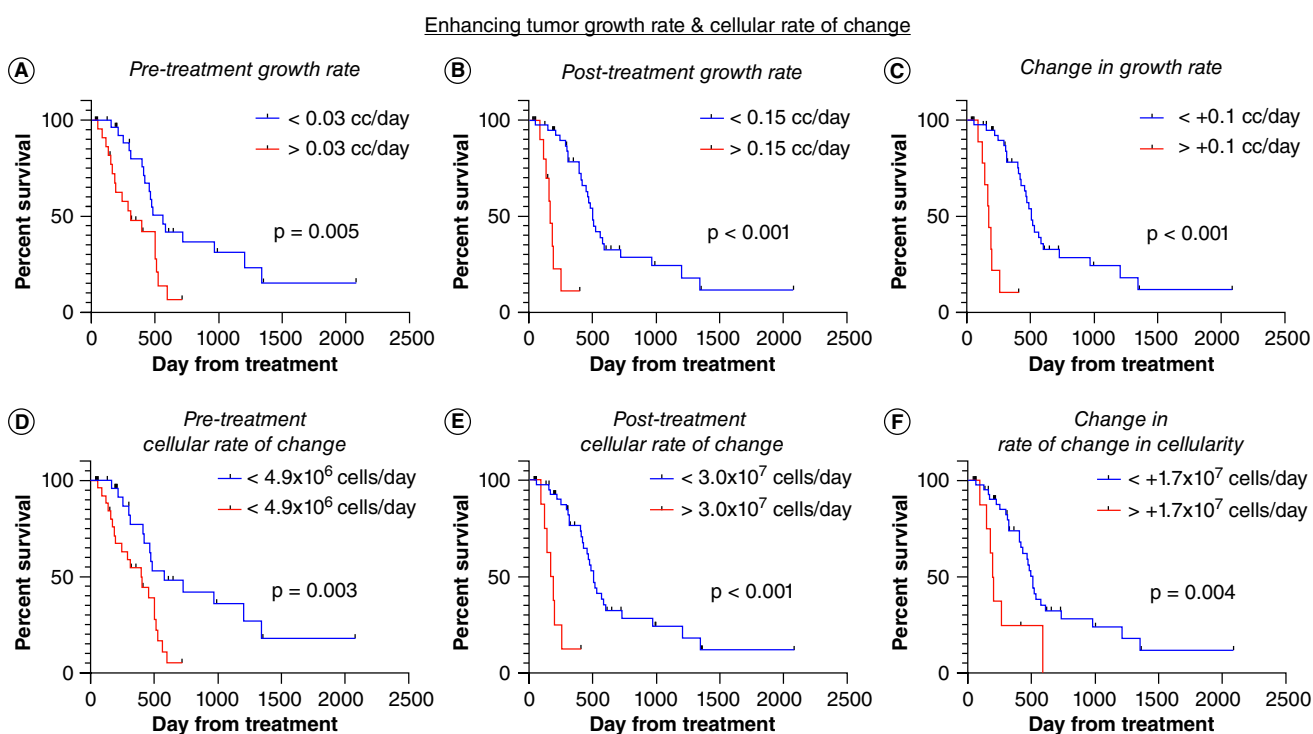
Figure 5. Kaplan-Meier curves for overall survival stratified by volumetric growth rate or the rate of change in cellularity. Patients with smaller pre-treatment **(A & D)** growth or cellular rates of change, **(B & E)** post-treatment growth or cellular rate of change, or **(C & F)** a larger *decrease* in growth rate or cellular rate of change had significantly longer OS.

therapies often used as a reference or control arm in clinical trials. As theorized, both the volume of contrast enhancing tumor and the total cellularity defined as the summation of cell density across the entirety of the enhancing tumor at baseline and the 1st post-treatment time point were prognostic for survival. This is consistent with previous data demonstrating the contrast enhancing tumor contains the most cellular and dense regions of the tumor [25] and consistent with the overwhelming data suggesting contrast enhancing tumor is,

for the most part, a strong surrogate underlying tumor burden [24,26]. However, it should be noted that anti-angiogenic therapies, immunotherapies and other novel treatments may not induce the same changes in cell density as cytotoxic agents, as the mechanism of action for cytotoxic agents directly impacts TPM parameters such as cellularity and ECF. Future studies should investigate the utility of TPM across various therapeutic approaches to assess its broader applicability as a predictive biomarker. This will be essential to determining whether the radio-

pathomic model can be generalized beyond traditional cytotoxic regimens and used to evaluate responses to newer, targeted therapies.

Additionally, our data demonstrate that both the rate of change in total enhancing tumor size as well as total estimated cellularity *after* treatment, in addition to the rate of change in volume and cellularity, are strong predictors of survival in patients with recurrent glioblastoma treated with cytotoxic treatments. While we previously showed a decrease in enhancing tumor volumetric growth rates after treatment were associated with a prolonged survival in an overlapping patient cohort [24], the current results including radio-pathomic map data appears to suggest this may be due to the enhancing tumor reflecting the majority of cellularity in recurrent glioblastoma.

Importantly and consistent with previous observations [17], some radio-pathomic maps showed regions of hypercellularity outside the areas of contrast enhancement likely representing non-enhancing tumor. While non-enhancing tumor volume of GBM can impact OS [27], overwhelming data suggests the enhancing tumor has the highest density and current response criteria recommend ignoring areas of suspected tumor outside of contrast enhancement due to difficulty distinguishing tumor from other mechanisms that influence T_2/FLAIR signal in gliobastoma including post-radiation changes, post-surgical changes, vasogenic edema [7]. Regardless, further investigation into the added value of including cellularity within the T_2 hyperintense regions is warranted.

The present study has several limitations. First, not every case in our dataset had the *IDH* mutation status confirmed because a large number of cases occurred before the *IDH* mutant subtype was identified. However, all patients were pathologically confirmed as WHO grade IV at the time of diagnosis, which included histologic features of traditional glioblastoma including vascular proliferation, high mitotic index and pseudopalisading necrosis. Nevertheless, it is possible that some *IDH* mutant gliomas were present and that they had an effect on both OS and imaging response. The diverse image acquisition protocol presents another limitation. Data included in the current study dated back to 2004, before the current acquisition recommendations [5,11], so this may have led to under-estimation of the model's performance and erroneous results. Importantly, we noticed systemic differences in cellularity that were dependent on the acquisition parameters and characteristics of the T_2-weighted FLAIR images that were used at each time point. However, this variability better represents a more "real world" scenario of use in the neuro-oncology community and therefore confirms the robustness of this approach.

Additionally, while our study demonstrates that post-treatment tumor cellularity and ECF are significantly associated with OS, we acknowledge that these measurements may not fully capture all biological processes influencing long-term treatment durability. Other factors such as the chemistry of the tumor microenvironment, metabolic behavior, immune modulation and adaptive resistance mechanisms likely play critical roles, particularly in the context of newer therapies such as immunotherapy or targeted treatments. Lastly, our study didn't compare the radio-pathomic model results with other advanced imaging techniques for depicting the pathologic features of GBM, such as perfusion MRI, pH-weighted chemical exchange saturation transfer echo-planar imaging, or amino acid PET. Future studies will be necessary to either compare or integrate the current radio-pathomic model with these techniques.

5. Conclusion

The current study utilized a radio-pathomic machine learning algorithm trained to map MRI characteristics to histological features to evaluate the response characteristics of recurrent glioblastoma patients treated with cytotoxic therapies. Results suggest smaller initial tumor volume, reduction in growth rate, smaller total cellularity, reduction in the rate of change in cellularity over time, as well as post-treatment cytoplasm and extracellular fluid density are predictive of survival.

Article highlights

- A "radio-pathomic" machine learning model was previously developed to estimate tumor cell density, cytoplasm density and extracellular fluid density from patient-specific MRI images and matching pathology at autopsy. However, it has not been evaluated as a tool for serial monitoring glioblastoma patients during treatment active treatment.
- This study revealed that smaller cytoplasm density and larger extracellular fluid density after treatment were associated with better survival, independent of tumor volume and other clinical factors, in patients with recurrent glioblastoma treated with cytotoxic chemotherapy with or without radiation.
- Post-treatment volumetric contrast enhancing growth rate on MRI and the rate of change in cellularity on radio-pathomic maps were independently associated with survival, suggesting this model may be a valuable tool for evaluating treatment response and predicting outcome in recurrent glioblastoma.

Competing interests disclosure

Writing disclosure

Ethical conduct of research

ORCID

Jingwen Yao https://orcid.org/0000-0002-8828-1841
Blaine S C Eldred https://orcid.org/0000-0002-3351-3895
Peter S LaViolette https://orcid.org/0000-0002-9602-6891
Benjamin M Ellingson
https://orcid.org/0000-0002-2764-6640

References

Papers of special note have been highlighted as: ●● of considerable interest

1. Alexander BM, Cloughesy TF. Adult glioblastoma. J Clin Oncol. 2017;35(21):2402–2409. doi:10.1200/JCO.2017.73.0119
2. Mandel JJ, Yust-Katz S, Patel AJ, et al. Inability of positive phase II clinical trials of investigational treatments to subsequently predict positive Phase III clinical trials in glioblastoma. Neuro Oncol. 2018;20(1):113–122. doi:10.1093/neuonc/nox144
3. Johnson DR, O'Neill BP. Glioblastoma survival in the United States before and during the temozolomide era. J Neurooncol. 2012;107(2):359–364. doi:10.1007/s11060-011-0749-4
4. Koshy M, Villano JL, Dolecek TA, et al. Improved survival time trends for glioblastoma using the SEER 17 population-based registries. J Neurooncol. 2012;107(1):207–212. doi:10.1007/s11060-011-0738-7
5. Ellingson BM, Bendszus M, Boxerman J, et al. Consensus recommendations for a standardized Brain Tumor Imaging Protocol in clinical trials. Neuro Oncol. 2015;17(9):1188–1198.
6. Ellingson BM, Wen PY, Chang SM, et al. Objective response rate targets for recurrent glioblastoma clinical trials based on the historic association between objective response rate and median overall survival. Neuro Oncol. 2023;25(6):1017–1028. doi:10.1093/neuonc/noad002
7. Wen PY, van den Bent M, Youssef G, et al. RANO 2.0: Update to the Response Assessment in Neuro-Oncology Criteria for High- and Low-Grade Gliomas in Adults. J Clin Oncol. 2023;41(33):5187–5199. doi:10.1200/JCO.23.01059
8. Wen PY, Macdonald DR, Reardon DA, et al. Updated response assessment criteria for high-grade gliomas: response assessment in neuro-oncology working group. J Clin Oncol. 2010;28(11):1963–1972. doi:10.1200/JCO.2009.26.3541
9. Ellingson BM, Wen PY, Cloughesy TF. Modified criteria for radiographic response assessment in glioblastoma clinical trials. Neurotherapeutics. 2017;14(2):307–320. doi:10.1007/s13311-016-0507-6
10. Okada H, Weller M, Huang R, et al. Immunotherapy response assessment in neuro-oncology: a report of the RANO working group. Lancet Oncol. 2015;16(15):e534–e542. doi:10.1016/S1470-2045(15)00088-1
11. Sanvito F, Kaufmann TJ, Cloughesy TF, et al. Standardized brain tumor imaging protocols for clinical trials: current recommendations and tips for integration. Front Radiol. 2023;3:1267615. doi:10.3389/fradi.2023.1267615
12. Ellingson BM, Harris RJ, Woodworth DC, et al. Baseline pretreatment contrast enhancing tumor volume including central necrosis is a prognostic factor in recurrent glioblastoma: evidence from single and multicenter trials. Neuro Oncol. 2017;19(1):89–98. doi:10.1093/neuonc/now187
13. Ellingson BM, Abrey LE, Nelson SJ, et al. Validation of postoperative residual contrast-enhancing tumor vol-

ume as an independent prognostic factor for overall survival in newly diagnosed glioblastoma. Neuro Oncol. 2018;20(9):1240–1250. doi:10.1093/neuonc/noy053

14. Ellingson BM, Wen PY, Cloughesy TF. Evidence and context of use for contrast enhancement as a surrogate of disease burden and treatment response in malignant glioma. Neuro Oncol. 2018;20(4):457–471. doi:10.1093/neuonc/nox193

15. Hygino da Cruz LC Jr, Rodriguez I, Domingues RC, et al. Pseudoprogression and pseudoresponse: imaging challenges in the assessment of posttreatment glioma. AJNR Am J Neuroradiol. 2011;32(11):1978–1985. doi:10.3174/ajnr.A2397

16. Thust SC, van den Bent MJ, Smits M. Pseudoprogression of brain tumors. J Magn Reson Imaging. 2018;48(3):571–589. doi:10.1002/jmri.26171

17. Bobholz SA, Lowman AK, Brehler M, et al. Radio-Pathomic Maps of Cell Density Identify Brain Tumor Invasion beyond Traditional MRI-Defined Margins. AJNR Am J Neuroradiol. 2022;43(5):682–688. doi:10.3174/ajnr.A7477
   •• This study was the first to describe development and construction of the "radio-pathomic" maps of cellularity and the first do demonstrate biologic accuracy.

18. Bobholz SA, Lowman AK, Connelly JM, et al. Noninvasive autopsy-validated tumor probability maps identify glioma invasion beyond contrast enhancement. Neurosurgery. 2024. doi:10.1227/neu.0000000000002898
   •• Demonstrates the biological accuracy of "radio-pathomic" maps in gliomas.

19. Bobholz SA, Hoefs A, Hamburger J, et al. Radio-pathomic maps of glioblastoma identify phenotypes of non-enhancing tumor infiltration associated with bevacizumab treatment response. J Neurooncol. 2024;167(2):233–241. doi:10.1007/s11060-024-04593-7

20. Abayazeed AH, Abbassy A, Mueller M, et al. NS-HGlio: a generalizable and repeatable HGG segmentation and volumetric measurement AI algorithm for the longitudinal MRI assessment to inform RANO in trials and clinics. Neurooncol Adv. 2023;5(1):vdac184. doi:10.1093/noajnl/vdac184

21. Cox RW. AFNI: software for analysis and visualization of functional magnetic resonance neuroimages. Comput Biomed Res. 1996;29(3):162–173. doi:10.1006/cbmr.1996.0014

22. Ellingson BM, Kim HJ, Woodworth DC, et al. Recurrent glioblastoma treated with bevacizumab: contrast-enhanced T1-weighted subtraction maps improve tumor delineation and aid prediction of survival in a multicenter clinical trial. Radiology. 2014;271(1):200–210. doi:10.1148/radiol.13131305

23. Ellingson BM, Gerstner ER, Smits M, et al. Diffusion MRI phenotypes predict overall survival benefit from anti-VEGF monotherapy in recurrent glioblastoma: converging evidence from Phase II trials. Clin Cancer Res. 2017;23(19):5745–5756. doi:10.1158/1078-0432.CCR-16-2844

24. Oshima S, Hagiwara A, Raymond C, et al. Change in volumetric tumor growth rate after cytotoxic therapy is predictive of overall survival in recurrent glioblastoma. Neurooncol Adv. 2023;5(1):vdad084. doi:10.1093/noajnl/vdad084
   •• Demonstrated use of contrast enhancing tumor growth rate changes as a biomarker for predicting survival in recurrent glioblastoma treated with cytotoxic therapy. This was compared directly with the rate of change in cellularity using radio-pathomic maps in the current study.

25. Kelly KA, Kirkwood JM, Kapp DS. Glioblastoma multiforme: pathology, natural history and treatment. Cancer Treat Rev. 1984;11(1):1–26. doi:10.1016/0305-7372(84)90014-8

26. Auer TA, Della Seta M, Collettini F, et al. Quantitative volumetric assessment of baseline enhancing tumor volume as an imaging biomarker predicts overall survival in patients with glioblastoma. Acta Radiol. 2021;62(9):1200–1207. doi:10.1177/0284185120953796

27. Kotrotsou A, Elakkad A, Sun J, et al. Multi-center study finds postoperative residual non-enhancing component of glioblastoma as a new determinant of patient outcome. J Neurooncol. 2018;139(1):125–133. doi:10.1007/s11060-018-2850-4